



REPORT DOCUMENTATION PAGE

Form Approved
OMB No 0704-0188

(2)

Public reporting burden for this collection of information is estimated to average 1 hour per response, including the time for reviewing instructions, searching existing data sources, gathering and maintaining the data needed, and completing and reviewing the collection of information. Send comments regarding this burden estimate or any other aspect of this collection of information, including suggestions for reducing this burden, to Washington Headquarters Services, Directorate for Information Operations and Reports, 1215 Jefferson Davis Highway, Suite 1204, Arlington, VA 22202-4302, and to the Office of Management and Budget, Paperwork Reduction Project (0704-0188), Washington, DC 20503.

1. AGENCY USE ONLY (Leave blank)		2. REPORT DATE 31 Dec 93	3. REPORT TYPE AND DATES COVERED Final 1 May 92 - 31 Oct 93	
4. TITLE AND SUBTITLE Dynamic Response of Ceramics			5. FUNDING NUMBERS DAAL03-92-G-0218	
6. AUTHOR(S) Thomas J. Ahrens, Guangqing Chen, and James A. Tyburczy			  PERFORMING ORGANIZATION REPORT NUMBER FEB 09 1994	
7. PERFORMING ORGANIZATION NAME(S) AND ADDRESS(ES) Lindhurst Laboratory of Experimental Geophysics Seismological Laboratory 252-21 California Institute of Technology Pasadena, CA 91125				
8. SPONSORING MONITORING AGENCY NAME(S) AND ADDRESS(ES) U.S. Army Research Office P. O. Box 12211 Research Triangle Park, NC 27709-2211			9. SPONSORING MONITORING AGENCY REPORT NUMBER ARO 28884.5-MS	

11 SUPPLEMENTARY NOTES
The views, opinions and/or findings contained in this report are those of the author(s) and should not be construed as an official Department of the Army position, policy, or decision, unless so designated by other documentation.

12a DISTRIBUTION AVAILABILITY STATEMENT
Approved for public release; distribution unlimited.

12b DISTRIBUTION CODE

94-04455



13. ABSTRACT (Maximum 200 words) **94 2 08 155**

Both solid to gas ($\text{CaSO}_4 + \text{SiO} \rightarrow \text{CaSiO}_3 + \text{SO}_2$ and $\text{Si}_3\text{N}_4 + 3\text{C}$ (diamond) \rightarrow and $3\text{SiC} + 2\text{N}_2$) can be shock-induced at ballistic velocities. Because of the endothermic nature of the gas-producing reactions, the extent of reactions observed are limited to interfaces. We found the above reactions proceed to a much less extent than calculation by equilibrium thermodynamic calculations. Reaction products are found to be 10^{-2} times those calculated for equilibrium. We show that the extent of reaction, rather than limited by the usual diffusion processes appears to be controlled by dynamic mixing processes arising from Rayleigh-Taylor instabilities at, for example, $\text{CaSiO}_4\text{-SiO}_2$ interfaces. We apply a theory developed by Drucker [1] to account for the observed extent of reaction.

14 SUBJECT TERMS Gas-producing reactions, shock chemistry, Rayleigh-Taylor instabilities		15. NUMBER OF PAGES	
		16. PRICE CODE	
17 SECURITY CLASSIFICATION OF REPORT UNCLASSIFIED	18 SECURITY CLASSIFICATION OF THIS PAGE UNCLASSIFIED	19 SECURITY CLASSIFICATION OF ABSTRACT UNCLASSIFIED	20 LIMITATION OF ABSTRACT UL

AD-A275 396



CALIFORNIA INSTITUTE OF TECHNOLOGY

SEISMOLOGICAL LABORATORY 252-21

December 28, 1993

Effect of Gas Producing Reactions on Stress Wave Propagation

FINAL REPORT

Thomas J. Ahrens, G. Chen, and James A. Tyburczy

U.S. Army Research Office

DAAL03-92-G-0218

(CIT 64562)

Accession For		
NTIS	CRA&I	<input checked="" type="checkbox"/>
DTIC	TAB	<input type="checkbox"/>
Unannounced		<input type="checkbox"/>
Justification		
By		
Distribution/		
Availability Codes		
Dist	Availability for special	
A-1		

APPROVED FOR PUBLIC RELEASE;
DISTRIBUTION UNLIMITED

DTIC QUALITY INSPECTED 5

The views, opinions, and/or findings contained in this report are those of the author(s) and should not be construed as an official Department of the Army position, policy, or less so designated by other documentation.

TABLE OF CONTENTS

List of Figures
List of Tables
List of Publications
Report of inventions (none)
List of all participating scientific personnel

	Page
Abstract	
1 Introduction.....	1
2 Gas-producing reactions.....	2
2.1 Reaction between silica and anhydrite.....	4
2.1.1 SEM instrument resolution.....	8
2.1.2 Mixing of sulfate with silica.....	13
2.1.3 Degree of devolatilization.....	16
3 Conclusions.....	20
References.....	20

LIST OF FIGURES

<u>Figure</u>		<u>Page</u>
1:	SEM micrograph of shot 1100. Light area is Si_3N_4 , voids where diamond grains plucked out indicate weak bonding.	5
2:	SEM micrograph of shot 1106. Darker area is quartz, lighter area anhydrite.	5
3a:	SEM micrograph of shot 1099 near sample edge. Dark gray area is SiO , light gray area is $\text{Ca}_4\text{Si}_3\text{SO}_{13}$. Black area is epoxy.	5
3b:	Shot 1099 away from edge. Large grains are SiO , fine-grained material is CaSO_4 .	5
4.	X-ray diffraction spectra of silica-anhydrite mixture before- and after-shock (Shot #1109, 42.3 GPa). The two spectra at bottom are JCPDS standards for CaSO_4 and SiO_2 . Molar ratio of silica to anhydrite is 3:1. Initially crystalline quartz is amorphized in the after-shock material.	9
5.	Atomic ratio of Ca/O profiles of three recovery shots on calcium sulfate and quartz. A cold pressed sample was used to estimate SEM resolution. Theoretical fits are given by Equation 12 with parameters: (1) dashed curve: $l = 0.53 \mu\text{m}$, $L = 0$; (2) solid curve: $l = 0.53 \mu\text{m}$, $L = 1.5 \mu\text{m}$. The data at $1 \mu\text{m}$ on the dashed curve represent three analyses at different locations near the boundary.	11
6.	Atomic ratio of S/Ca profiles of recovery shots on calcium sulfate and quartz. Solid curve is given by Equation 14. Further into SiO_2 , S/Ca ratio becomes indeterminate and is indicated by the dashed line. Error bars represent SEM analytical uncertainty. Results for other 20 mm shots are similar and not shown.	12
7.	Degree of devolatilization via reactions (A) and (B) as a function of shock pressure. The curves are calculated using Equations 16-21. Partial pressures of O_2 and SO_2/SO_3 are taken to be 0.2 and 10^{-4} bar, respectively, in the calculation, which are representative values for normal atmosphere. Impact velocities are indicated for shock pressures of 20, 40, 60, and 80 GPa.	19

LIST OF TABLES

<u>Table</u>		<u>Page</u>
1:	Recovery experiments on three gas-producing reactions	3
2:	Equation-of-state constants of anhydrite, silicate and their mixture.	7

List of Publications:

Effect of gas-producing and polymorphic reactions on stress wave propagation, Thomas J. Ahrens and Guangqing Chen, Proceedings of the Army Symposium on Solid Mechanics, August 17-19, 1993, Plymouth, MA.

Shock-induced devolatilization of calcium sulfate and implications for K-T extinctions, Guangqing Chen, James A. Tyburczy, and Thomas J. Ahrens, submitted to *Earth Planet. Sci. Lett.*

List of Participating Scientific Personnel

Thomas J. Ahrens

James A. Tyburczy

Guangqing Chen

Effect of gas-producing reactions on stress wave propagation

Thomas J. Ahrens, Guangqing Chen, and James A. Tyburczy*
*Lindhurst Laboratory of Experimental Geophysics, Seismological Laboratory,
California Institute of Technology, Pasadena, CA 91125*

December 29, 1993

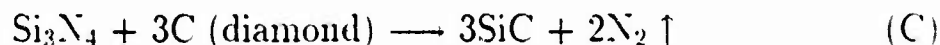
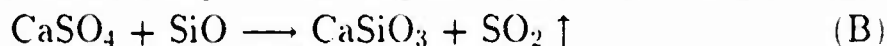
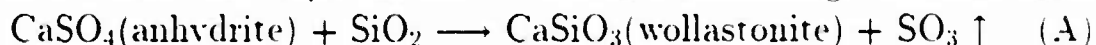
Abstract

Both solid to gas ($\text{CaSO}_4 + \text{SiO} \rightarrow \text{CaSiO}_3 + \text{SO}_2$ and $\text{Si}_3\text{N}_4 + 3\text{C}$ (diamond) \rightarrow and $3\text{SiC} + 2\text{N}_2$) can be shock-induced at ballistic velocities. Because of the endothermic nature of the gas-producing reactions, the extent of reactions observed are limited to interfaces. We found the above reactions proceed to a much less extent than calculation by equilibrium thermodynamic calculations. Reaction products are found to be 10^{-2} times those calculated for equilibrium. We show that the extent of reaction, rather than limited by the usual diffusion processes appears to be controlled by dynamic mixing processes arising from Rayleigh-Taylor instabilities at, for example, CaSiO_4 - SiO_2 interfaces. We apply a theory developed by Drucker [1] to account for the observed extent of reaction.

* Also at Department of Geology, Arizona State University, Tempe, AZ 85287

1 Introduction

Shock-induced endothermic solid-solid phase changes and gas-producing reactions have been studied in material consolidation and synthesis, especially starting with powdered materials (e.g.[2, 3, 4, 5]). Although thermal effects induced by shock compression is the major factor inducing chemical reactions under dynamic stress loading, unloading within the time scale of microseconds can be expected to proceed very differently than under equilibrium conditions. Gas-producing reactions, as well as solid-solid phase changes involving large density changes with their potential effects on partitioning of linear momentum, may have some ballistic application. Particularly, we have examined the following three reactions:



2 Gas-producing reactions

A series of recovery experiments and bulk chemical analyses were conducted on the recovered samples. No (solid) reaction products are found for reactions (1) and (2), but reaction (3) is discovered to take place to a varied extent in different shots. These results contradict Gibbs' formation energy calculations, which allow all three reactions to proceed below calculated after-shock temperatures.

The shock experiments utilize a 20 mm gun at Caltech's Shock Wave Lab. Reactants (in powder form, particle sizes 10-30 μm , except Si_3N_4 is whisker shaped) are mixed and pressed in 304 stainless steel containers. The sample chambers are usually evacuated to 30 millitorr until just before the shots are fired. The shot parameters are listed in Table 1. Flyer plates are tantalum unless specified otherwise in parentheses. Hugoniot pressures are calculated following the formulation outlined by Yang *et al.* [5] assuming 100% crystal density, actual reflected pressures are higher, but non-uniform.

Table 1: Recovery experiments on three gas-producing reactions

Starting mix (wt. %)	Initial density (%)	Shot number	Flyer plate velocity (km/s)	Pressure (GPa)
-------------------------	---------------------------	----------------	--------------------------------	-------------------

Si ₃ N ₄	diamond				
16	84	65	953	1.93	41.9
16	84	70	961	1.95	42.5
20	80	66.6	962	1.97	43.0
16	84	55.5	968	1.96	42.9
16	84	60	971	1.90 (SS 304)	43.5
16	84	65	1095	1.90	41.2
16	84	65	1096	1.69	35.9
16	84	65	1097	1.98	43.2
80	20	60	1100	1.82	35.8

CaSO ₄	SiO ₂				
69	31	83	1106	1.87	33.8
69	31	70	1107	2.02 (W)	42.2
69	31	60	1108	1.92	35.0
38	62	61	1109	1.90	42.3
87	13	78	1110	1.94	32.5
69	31	79	1111	1.89	34.3
69	31	77	1112	1.88	34.1
69	31	72	917 (40mm gun)	1.59	27.4
69	31	73	923 (40mm gun)	1.77	31.5

CaSO ₄	SiO				
67	33	89	1098	2.06 (W)	
67	33	82	1099	1.58	

Note: Flyer plate is Ta unless noted otherwise.

Using reactant Hugoniot release paths (assuming the main part of the reaction takes place during the late stage of release), the calculated average after-shock temperatures are 2700-3000°C; for shot 1100, because of the inverted mass ratio, the same temperature for shot 1106 is 1200°C. Recovered samples are analyzed with SEM, electron microprobe, and x-ray diffraction. The SEM micrographs of shots for which reaction (1) was studied (Fig. 1) show Si_3N_4 is molten after shock, but diamond is intact. Although in some small regions near boundaries of the two reactants decrease in nitrogen K_α x-ray intensity relative to silicon intensity is detected, it is believed to be an effect of geometric absorption by neighboring carbon atoms. All prominent peaks in XRD spectra are identified with diamond/ Si_3N_4 peaks, therefore the reaction product must be lower than the detection limit (about 2%), and gas production is not enough to account for the sample holder explosions reported by Yang *et al.* For shot 1066, reaction (2) does not occur, but an interesting feature is discovered in the sample: quartz grains apparently became molten but anhydrite did not (Fig. 2) despite SiO_2 's higher melting point (1500°C vs. CaSO_4 's 1400°C).

In comparison to the inert reactions (1) and (2), reaction (3) is quite active. The bulk reaction product (CaSiO_4) yield is estimated at about 30% for shot 1098. Reduction of a factor of 4-5 in sulfur content is seen while calcium is unchanged, and the deficit in atomic number is approximately made up with incorporation of silicon which demonstrates the importance of SiO participation. To find the initiation of the reaction, shot 1099 was conducted at a lower pressure. Clearly separated reaction and no-reaction zones are seen in the SEM micrographs (Figs. 3a, b). Both materials appear to have been molten. In the no-reaction zones, there may be some melting in SiO, especially at grain boundaries, but CaSO_4 remains solid during compression. Like quartz, SiO also has a higher melting point (1700°C) than CaSO_4 .

2.1 Reaction between silica and anhydrite

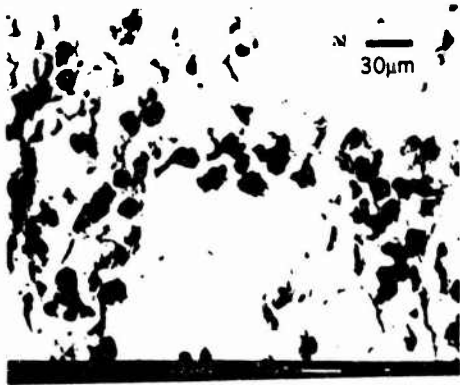


Fig. 1: SEM micrograph of shot 1100. Light area is Sb_3N_4 , voids where diamond grains plucked out indicate weak bonding. TJA93133SFD

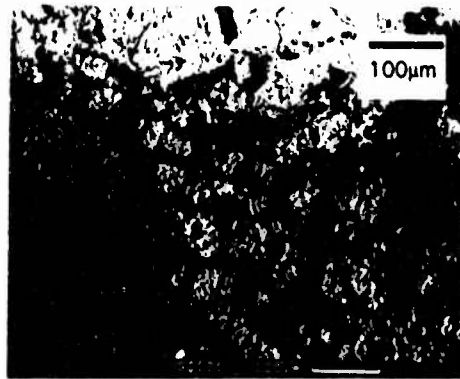


Fig. 2: SEM micrograph of shot 1106. Darker area is quartz, lighter area anhydrite. TJA93134SFD



Fig. 3a: SEM micrograph of shot 1099 near sample edge. Dark gray area is SiO_2 , light gray area is $Ca_3Si_3SO_{13}$. Black area is epoxy. TJA93135SFD

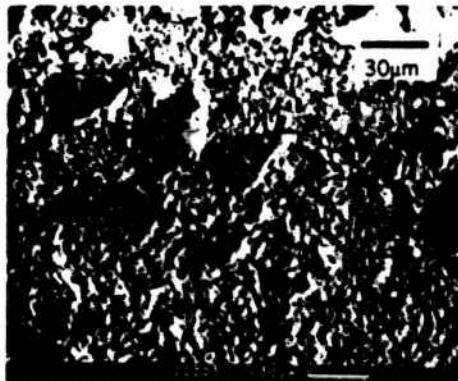


Fig. 3b: Shot 1099 away from edge. Large grains are SiO_2 , fine-grained material is $CaSO_4$. TJA93136SFD

Experimental parameters are listed in Table 1 (two shock experiments on anhydrite/SiO are listed and will be discussed later). The starting material was a mixture of silica (crystalline or amorphous, Alfa #13024 and 89709) and natural crystalline anhydrite (Ward's Geology #46E0535) powders and was pressed into target container to initial densities of 60–85% of its Archimedian density. Average silica grain size was 4 μm , and anhydrite grains were mostly between 30–100 μm . Equation-of-state constants for the mixture (see Table 2) were calculated from previous anhydrite data of Simakov *et al.*[8] and quartz data of Swegle *et al.*[9] using the formulae by Boslough [2]: assuming uniform stress distribution, for a two-component system.

$$V = m_1 V_1 + m_2 V_2. \quad (1)$$

$$K_{0S} = [(v_1/K_{0S1}) + (v_2/K_{0S2})]^{-1}. \quad (2)$$

$$K'_{0S} = K_{0S}^2 [v_1(1 + K'_{0S1})/K_{0S1}^2 + v_2(1 + K'_{0S2})/K_{0S2}^2] - 1. \quad (3)$$

where m_i , V_i , v_i , K_{0Si} and K'_{0Si} are the components' mass fractions, specific volumes, initial volume fractions, bulk moduli and their pressure derivatives at zero pressure. Shock pressures determined by impedance-match method range from 27.4 to 42.3 GPa. Five 20 mm shots and the two 40 mm shots (see Table 1) all had 1:1 molar ratio of anhydrite : silica. The initial porosity of the mixture were 17.2% (1106) to 40.0% (1108): Shot 1107 employed fused quartz: The 40 mm shots were conducted to determine the shock duration effect on the reaction, but no reaction was seen in shot 917, and shot 923 was not recovered: Finally, shots 1109 and 1110 had anhydrite : silica molar ratios of 1:3.7 and 3.0:1. Recovered samples were analyzed with petrographic microscopy, scanning electron microscopy (SEM, instrument: Camscan Series 2 with Tracor Northern EDS detector TH-3/54-6901, operated at 15 kV) and X-ray diffraction (XRD, instrument: Scintag DMC-008, radiation source: Cu-K α). Compared with the original material, the changes exhibited in the 20 mm (except shot 1111, which will be described separately in

Table 2. Equation-of-state constants of
anhydrite, silica and their mixture.

Material	ρ (g/cm ³)	K_{0S} (GPa)	K'_{0S}
Anhydrite (LPP)	2.97	38.5	6.0
Silica (HPP)	4.29	350	3.3
Mixture (1:1 molar)	3.28	48.7	7.6

the following paragraph) post-shock samples are quite similar: in agreement with previous research [10], silica becomes amorphous in spite of its original crystallinity (see XRD spectra in Figure 4; Anhydrite is recovered as a crystalline phase. Although shock-induced mosaicism in the crystal grains was observed with cross-polarized light on petrographic microscope, it appears unlikely that anhydrite recrystallized from a melt as no rounding of the grains was observed (see Figure 2).

In shot 1111 (in which 10 mass% iron powder was intentionally mixed in addition to anhydrite/quartz), devolatilization was much more extensive than the rest of the shots and reaction of iron to iron sulfate and iron sulfide were observed. In their study of sulfur speciation in basaltic glasses [11], Carroll and Rutherford reported that proportion of dissolved sulfur present as sulfate (as opposed to sulfide) increases from near 0% at FMQ (fayalite-magnetite-quartz) oxygen fugacity to near 100% at 2 to 3 $\log f_{O_2}$ units above FMQ. The oxygen fugacity present in these recovery experiments was well into the sulfate stable regime. The presence of iron sulfide led us to believe the greater degree devolatilization of $CaSO_4$ within 1 mm of the stainless steel container in all the 20 mm shots was affected by the reducing effect of the metal and would not have occurred in its absence. In the central metal-free region, the dimensions of possible reaction zones are so limited that they were nearly at the limit of spatial resolution of the SEM. In the following three sections we will attempt to derive the actual degree of devolatilization from experimentally observed chemical compositions at different locations in the samples.

2.1.1 SEM instrument resolution

The SEM electron beam spot is much less than $1\mu m$, but the dimension of excitation volume in the sample, and therefore the instrument resolution, is larger due to electron scattering and secondary fluorescence in the sample [12]. A "smearing" function is assumed to convolve with

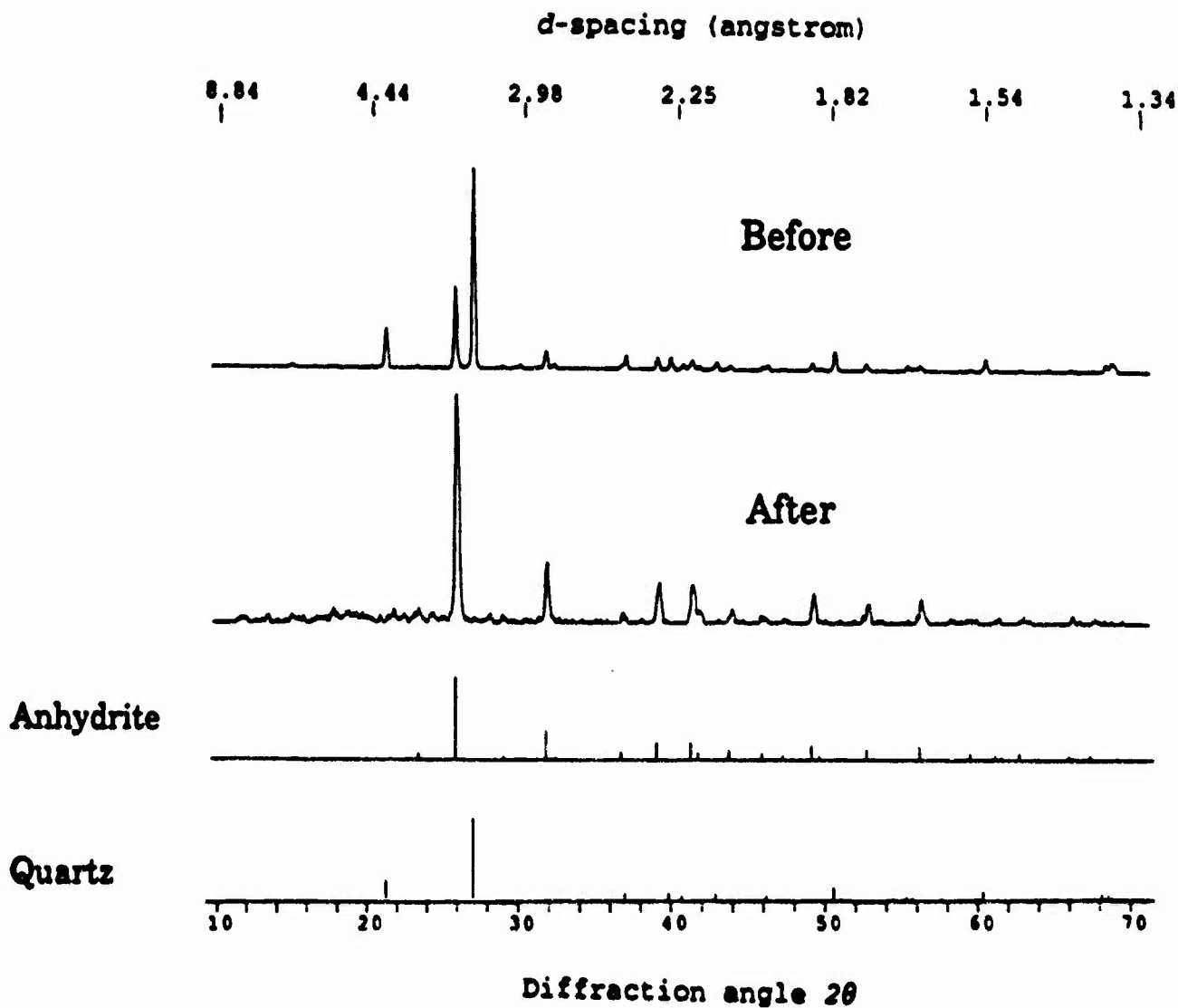


Fig. 4. X-ray diffraction spectra of silica-anhydrite mixture before- and after-shock (Shot #1109, 42.3 GPa). The two spectra at bottom are JCPDS standards for CaSO_4 and SiO_2 . Molar ratio of silica to anhydrite is 3:1. Initially crystalline quartz is amorphized in the after-shock material.

the "true" chemical composition to give the observed composition. The function form is taken to be Gaussian:

$$f(x) = \frac{1}{\sqrt{\pi}l} \exp(-x^2/l^2), \quad (4)$$

$$\int_{-\infty}^{\infty} f(x)dx = 1 \quad (5)$$

where $2l$ is a measure of spatial resolution. Anhydrite and quartz disks of ~ 1 mm thickness each were sandwiched together and heated at 573 K for 6 hours, followed by a 24-hour press at ~ 4000 psi so that plastic flow may take place to produce a good contact (with less-than-1 μm gap) as a no-reaction reference. A comparison between the SEM analysis across the pressed boundary and calculation (convolution of Equation 4 and a step function) found $l = 0.53\mu\text{m}$ to provide the best fit (Figure 5). This agrees with our expectation that the resolution distance is larger than the electron beam diameter.

The data in Figures 5 and 6 are corrected for secondary fluorescence excited by characteristic radiations. Another concern has been the fluorescence excited by the continuous spectrum. We use an approximate equation ((15.10) in Reed [13]), modified for compounds by multiplying the ratio of mass attenuation coefficients of the excited element A (μ_C^A) and the compound (μ_C), the intensity of fluorescence I_f relative to electron-excited characteristic K-radiation of element A in the compound I_C^A is thus

$$\frac{I_f}{I_C^A} = 9.7 \times 10^{-8} Z^4 \frac{\mu_C^A}{\mu_C}, \quad (6)$$

(Z is the atomic number of the excited element). The correction factor for continuum fluorescence is

$$F_f = 1 / (1 + \frac{I_f}{I_C^A}). \quad (7)$$

We consider three cases:

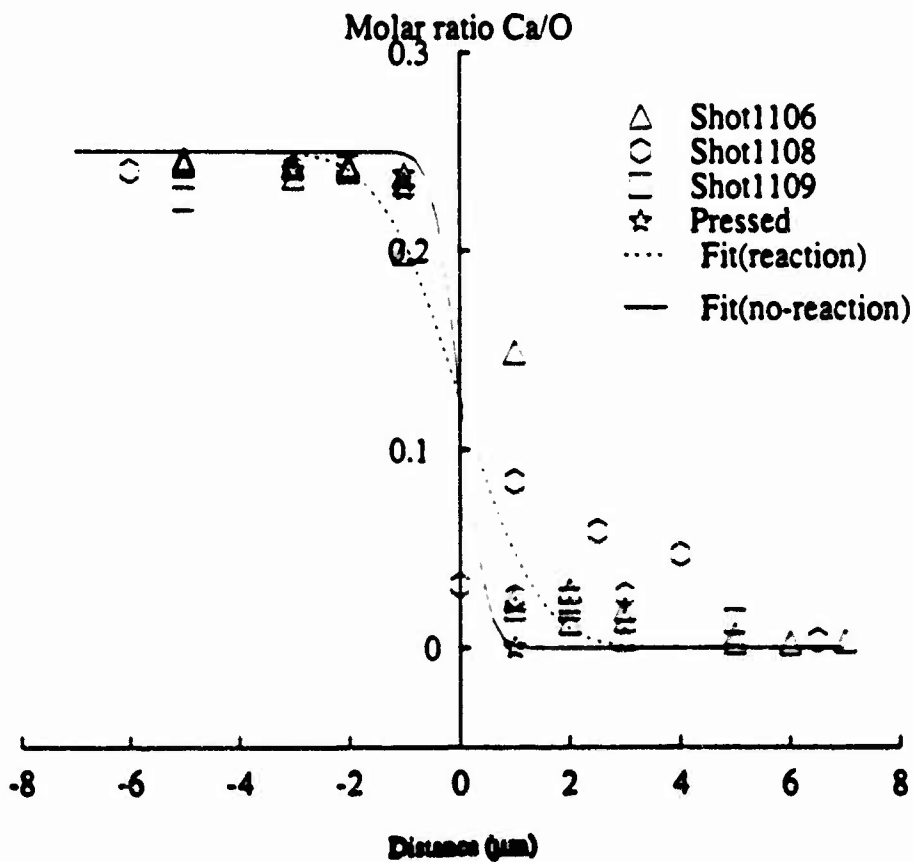


Fig. 5. Atomic ratio of Ca/O profiles of three recovery shots on calcium sulfate and quartz. A cold pressed sample was used to estimate SEM resolution. Theoretical fits are given by Equation 12 with parameters: (1) dashed curve: $l = 0.53 \mu\text{m}$, $L = 0$; (2) solid curve: $l = 0.53 \mu\text{m}$, $L = 1.5 \mu\text{m}$. The data at $1 \mu\text{m}$ on the dashed curve represent three analyses at different locations near the boundary.

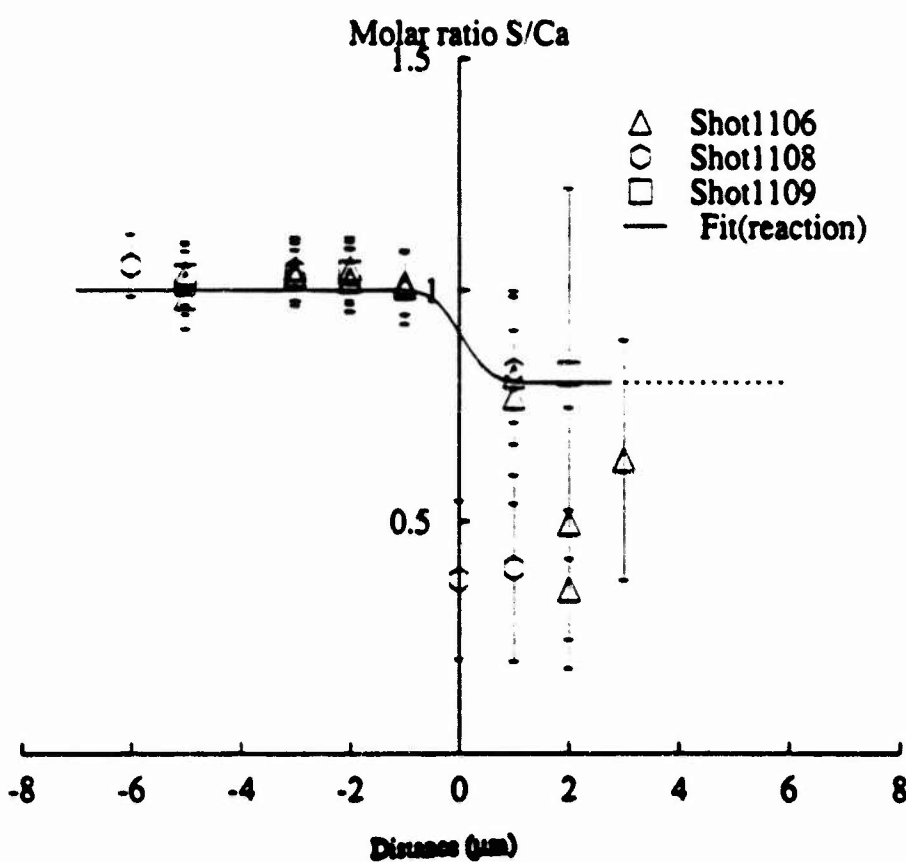


Fig. 6. Atomic ratio of S/Ca profiles of recovery shots on calcium sulfate and quartz. Solid curve is given by Equation 14. Further into SiO_2 , S/Ca ratio becomes indeterminate and is indicated by the dashed line. Error bars represent SEM analytical uncertainty. Results for other 20 mm shots are similar and not shown.

1. Compound is 50 mol.% CaSO₄ and 50 mol.% SiO₂ (in the middle of the mixing zone), $I_f^{Ca}/I_C^{Ca}=1.21\%$, $I_f^S/I_C^S=0.24\%$;
2. Compound is near 100% SiO₂ with a trace of Ca and S (deep into silica). $I_f^{Ca}/I_C^{Ca}=0.67\%$, $I_f^S/I_C^S=0.13\%$;
3. A sharp CaSO₄-SiO₂ boundary, with the electron beam shifted to SiO₂ side so that the electron-excitation volume is completely in SiO₂. Any Ca and S signal is purely due to secondary fluorescence from the SiO₂ continuum (Si characteristic line is not energetic enough to excite Ca or S). The secondary fluorescence intensity, relative to electron-excited radiation in pure CaSO₄, is given by:

$$\frac{I_f^{Ca,S}}{I_{CaSO_4}^{Ca,S}} = 0.5 \times 9.7 \times 10^{-8} Z^4 \frac{\mu_{CaSO_4}^{Ca,S}}{\mu_{CaSO_4}} \quad (8)$$

Equation 8 is very similar to Equation 6 except the factor 0.5, which arises because only half of the continuous radiation goes into CaSO₄, neglecting the finite width of the primary X-ray source. The ratios for Ca and S calculated are 0.23% and 0.11%.

More detailed numerical calculations were done and the results agree within $\pm 0.3\%$. Case (3) agrees very well with observations at 1 μm in quartz from the cold-pressed boundary, where Ca and S signal intensities are $0.2 \pm 0.1\%$ and $0.4 \pm 1\%$ of those in pure CaSO₄ (Figure 5). For the shock-recovered samples, the Ca and S intensities within $\sim 3\mu\text{m}$ from the boundaries are much higher than the secondary fluorescence level and the corrections are negligible compared to the analytical uncertainty.

2.1.2. Mixing of sulfate with silica

In shocked samples the boundary layer between calcium sulfate and silica is thicker than the cold-pressed edge. In the following we examine several possible mixing mechanisms:

1. Solid state diffusion:

The diffusion constants of H, ^{18}O and ^{30}Si atoms in quartz have been documented in [14]. At 800°C , they vary over a wide range, with H having the highest $D = 2.5 \times 10^{-11} \text{ m}^2/\text{s}$. and ^{30}Si having the lowest $D = 1.3 \times 10^{-21} \text{ m}^2/\text{s}$. In the time scale of our experiments $\sim 1\mu\text{s}$, the characteristic distance $\sqrt{Dt} \sim 10^{-8}-10^{-2}\mu\text{m}$ is much smaller than the observed reaction zone thickness:

2. Liquid state diffusion:

Rubie *et al.* directly measured oxygen self-diffusivity in $\text{Na}_2\text{Si}_4\text{O}_9$ melt up to 1825°C and between 4–10 GPa [15]. The diffusion constant they reported ranges from 1.0 to $4.2 \times 10^{-10} \text{ m}^2/\text{s}$ increasing with temperature and pressure. Si-O bond breaking is the basic process controlling both O self-diffusion in $\text{Na}_2\text{Si}_4\text{O}_9$ and CaSO_4 diffusion in silica melt which is of present interest. It is possible to use these data to obtain an order-of-magnitude estimate of mixing time and length scales in the SiO_2 liquid. Again, in the $1\mu\text{s}$ shock duration, the highest diffusivity ($4.20 \times 10^{-10} \text{ m}^2/\text{s}$) gives characteristic distance $2 \times 10^{-2}\mu\text{m}$, which is still too small to account for the μm -size mixing layer:

3. Rayleigh-Taylor instability:

Although initially crystalline quartz is amorphized during shock, we cannot conclude that it has been once molten because quartz can transform to diaplectic glass without melting [10]. Since there is a strong contrast in strength of quartz and anhydrite (~ 1 GPa for quartz and ~ 0.1 GPa for anhydrite), we suggest Rayleigh-Taylor instability as the third mixing mechanism.

Rayleigh-Taylor instability arises at interfaces between two materials of different strength when they are strongly accelerated or decelerated along a direction perpendicular to their planar interface. According to the theoretical model by Drucker[1], when shock wave propagates from the stronger material into the weaker material, the interface

experiences alternating compressional and tensile stress due to perturbations (bumps) on material surface. When the stress difference exceeds the strength of the stronger material (σ_0), the bumps grow freely and instability occurs. Two important derivations of the theory are threshold perturbation amplitude:

$$h_0^{th} = H(1 + \pi/2)\sigma_0 F/P, \quad (9)$$

and time dependence of instability growth above the threshold:

$$h - h_0^{th} = (h_0 - h_0^{th}) \cosh \sqrt{3Pt/(\lambda\rho H)}, \quad (10)$$

where H is material thickness. h_0 is initial perturbation amplitude. ρ is material density. P is shock pressure. λ is the perturbation wavelength. F is a geometric factor between 0.25-1, and $\beta = \frac{16}{(4+\pi)F} \sim 2-8$.

A prominent feature of the theory is that the threshold is independent of wavelength λ . Experiments by Barnes *et al.* on aluminum and 304 stainless steel plates support the theoretical prediction [16].

For our case, $\sigma_0 \sim 1$ GPa, $\rho=2.65$ g/cm³, $P=40$ GPa, $\lambda \sim H \sim$ grain size $4\mu\text{m}$, the threshold thickness perturbation calculated from Equation 9 is $\sim 0.4\mu\text{m}$, which is very reasonable. Above threshold, the growth is very fast: for an initial perturbation 10% above threshold, Equation 10 indicates that it takes a few nanoseconds to grow to sizes comparable to $\lambda/2$, after which the theory is no longer valid.

From the above discussion, Rayleigh-Taylor instability emerges as a plausible mechanism to drastically increase surface area at contact interface and at the same time reduce the distance material has to diffuse to mix efficiently. We thus propose the reaction to be Rayleigh-Taylor instability-driven, and only takes place at a later stage at solid-solid interfaces. Such reactions would have the following characteristics:

1. The amount of reaction is surface-limited and therefore independent of grain size, molar ratio, *etc.* of the reactants. This is consistent with our observation:

2. Rayleigh-Taylor instability as a mechanical process does not rely on compositional gradient, therefore reaction rates have a less important role in these reactions compared to in those driven by diffusion.

Although we propose the anhydrite-SiO₂ reaction is not dominantly a diffusive process, we mathematically describe the shocked sample interface by a linear diffusion profile. Denote $g_{Ca}(x)$ = the molar ratio of Ca/O, the solution of one dimensional diffusion equation (heat equation, see, e.g., [17]) with initial conditions:

$$g_{Ca}(x)|_{t=0} = \begin{cases} 0.25 & \text{if } x \leq 0 \\ 0 & \text{if } x > 0 \end{cases}$$

is

$$g_{Ca}(x) = \frac{1}{8} \operatorname{erfc}(x/L). \quad (11)$$

A fit to the shocked sample profile (convolved with $f(x)$) gives the mixing length $L \simeq 1.5 \mu\text{m}$ (solid line in Figure 5):

$$g_{Ca}^{SEM}(x) = \int_{-\infty}^{\infty} f(x-x') g_{Ca}(x') dx' \quad (12)$$

2.1.3 Degree of devolatilization

The experimentally seen devolatilization shows some scatter (Figures 5, 6). For simplicity, we assume an average of 20% S molar loss in the region $-L < x < L$, so the ratio S/O is

$$g_S(x) = 0.8 g_{Ca}(x) = 0.1 \operatorname{erfc}(x/L). \quad (13)$$

The S/Ca profile observed on SEM is given by

$$(S/Ca)(x) = \frac{\int_{-\infty}^{\infty} g_S(x') e^{-(x'-x)^2/L^2} dx'}{\int_{-\infty}^{\infty} g_{Ca}(x') e^{-(x'-x)^2/L^2} dx'}. \quad (14)$$

Bulk devolatilization, defined as the fraction of sulfur loss in the boundary layer over the total sulfur mass in the original sample, is given by

$$DV = \frac{3 \times \int_{-L}^L (g_{Ca} - g_S) dx}{g_{Ca}|_{x=-\infty} R} \quad (15)$$

where R is the anhydrite grain size. The factor 3 takes into account the three dimensional effect. For $R = 100 \mu\text{m}$, evaluation of the formula yields a numerical value of $DV = 6 \times 10^{-3}$.

We infer that anhydrite mixed into silica upon shock loading and underwent devolatilization during release. Tyburczy and Ahrens [7] used the following approach to calculate the extent of shock-induced reactions:

1. Entropy excess required for incipient reaction:

$$S_{IR} = \int_{T_0}^{T_{IR}} \frac{C_p}{T} dT, \quad (16)$$

where T_0 is room temperature. T_{IR} is the temperature of incipient reaction (at which the sums of Gibbs formation energies for the reactants and products are equal). C_p is the atmospheric pressure heat capacity at constant pressure.

2. Entropy excess required for complete reaction:

$$S_{CR} = S_{IR} + \Delta S - \sum_{\text{gas products}} n_i R \ln(P_i/P_0), \quad (17)$$

where ΔS is the entropy difference between reactants and products as computed from Robie *et al.* [6], the last term on the right takes into account effects of partial pressures, P_i , of gas products (P_0 is the ambient pressure), n_i is the number of moles of gas specie i , R is the gas constant ($8.31 \text{ J mol}^{-1} \text{ K}^{-1}$).

3. Entropy gain in the shocked state (and in the post-shock state assuming isentropic release):

$$\Delta S_H = S_{tr} + C_v \ln(T_H/T_S), \quad (18)$$

where S_{tr} is the entropy change of phase transition during compression. T_S is the temperature of isentropic compression from initial

volume V_0 at temperature T_i to Hugoniot volume V_H and isentropic pressure P_s :

$$T_s = T_i \exp \left[- \int_{V_0}^{V_H} \left(\frac{\gamma}{V} \right) dV \right] \quad (19)$$

where γ is the Grüneisen parameter. T_H is the shock temperature, determined by:

$$\frac{V_H}{\gamma} (P_H - P_s) = \int_{T_i}^{T_H} C_v dT \quad (20)$$

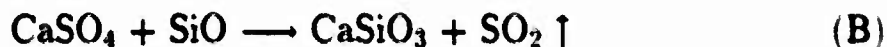
C_v is heat capacity at constant volume (at high pressure).

4. The extent of reaction is given by:

$$\text{Fraction of material reacted} = \frac{\Delta S_H - S_{IR}}{S_{CR} - S_{IR}}. \quad (21)$$

The results from Equation 21 for reaction (A) are shown as the solid and broken curves in Figure 7. The equation-of-state parameters are the same as in Table 2, and $S_{ir}=0$ for the calculation. Local devolatilization in the reaction layer is close to theoretical calculation, but decomposed anhydrite is only a small portion ($\sim 6 \times 10^{-3}$) of the total mass because of the dimension of the reaction layer is much smaller relative to the grain size ($\sim 100 \mu\text{m}$).

To examine the role of enthalpy difference in shock-induced reactions, we conducted two recovery experiments on anhydrite and amorphous silicon monoxide (SiO, Alfa #89430) powder mixture (Table 1). The reaction in question is



We observed extensive reaction in the recovered material of shot 1098, where S in anhydrite is reduced by a factor of 4-5. Although enthalpy of SiO glass is unknown, it is a less stable compound than quartz and therefore absorbs less energy in reaction (B). The weaker bonding structure compared to SiO_2 could also give rise to a much higher diffusion rate. Both may contribute to the excessive reaction which occurred.

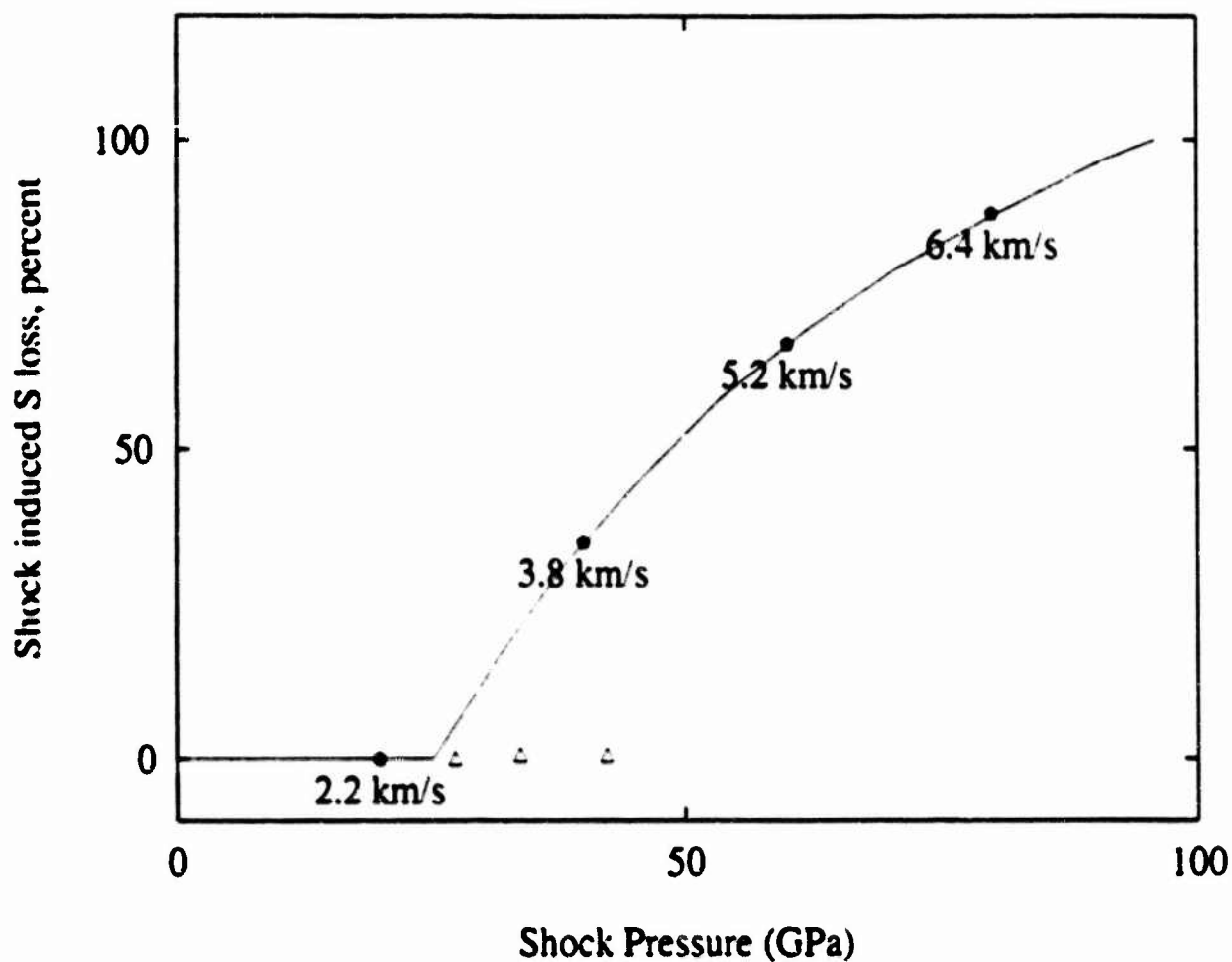
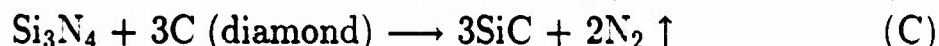
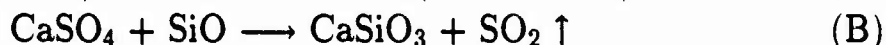
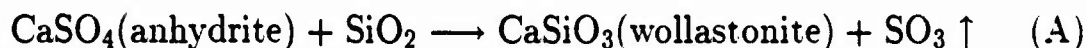


Fig. 7. Degree of devolatilization as a function of shock pressure of reaction $\text{CaSO}_4 + \text{SiO}_2 \rightarrow \text{CaSiO}_3 + \text{SO}_3 \uparrow$. The curves are calculated using Equations 16-21. Partial pressures of O_2 and SO_3 are taken to be 0.2 and 10^{-4} bar respectively in the calculation, which are representative values for normal atmosphere. Impact velocities are indicated for shock pressures of 20, 40, 60 and 80 GPa.

3 Conclusions

We studied three gas-producing solid-solid reactions under shock conditions:



The reactions are found to proceed only in a very limited reaction layer at the interfaces of the corresponding reactants, and for this reason, reacted portion of the material is a very small percent ($\sim 10^{-2}$) of the bulk, although inside the reaction zone, the extent of reaction can be much greater ($\sim 20\%$) and close to theoretical calculations.

With emphasis on reaction (A), we propose these reactions are controlled by the dynamic process of Rayleigh-Taylor instability instead of diffusion, as in reactions under equilibrium conditions. A model developed by Drucker is applied to anhydrite-SiO₂ interface. Since diffusion and reaction rates are secondary restraints for these reactions, such a mechanism explains the lower degree of reaction compared to equilibrium calculations observed in all three reactions.

Acknowledgments

We thank E. Gelle and M. Long for their help in performing the recovery experiments. Prof. Donald Burnett and Dr. John Armstrong provided valuable discussions on SEM analysis. TGA was performed in the Materials Preparation Facility in the Center for Solid State Science at Arizona State University.

References

- [1] D. C. Drucker, "Taylor Instability" of the Surface of an Elastic-Plastic Plate. *Mechanics Today*, V 5, Pergamon Press, New York (1975).

- [2] M. B. Boslough, A thermochemical model for shock-induced reactions (heat detonations) in solids. *J. Chem. Phys.* 92, 1839-1848 (1990).
- [3] H. Tan and T. J. Ahrens, Shock-induced polymorphic transition in quartz, carbon, and boron nitride, *J. Appl. Phys.* 67, 217-224 (1990).
- [4] D. J. Erskine and W. J. Nellis, *Nature*, 349, 317 (1991).
- [5] W. Yang, G. M. Bond, H. Tan, T. J. Ahrens, and G. Liu, Dynamic consolidation of super hard materials, *J. Mater. Res.*, 7, 1501-1518 (1992).
- [6] R. A. Robie, B. S. Hemingway and J. R. Fisher, Thermodynamic Properties of Minerals and Related Substances at 298.15K and 1 Bar (10^5 Pascals) Pressure and at Higher Temperatures. *U. S. Geol. Survey Bull.* 1452 (1979).
- [7] J. A. Tyburczy and T. J. Ahrens, Dynamic compression and volatile release of carbonates. *J. Geophys. Res.*, 91, 4730-4744 (1986).
- [8] G. V. M. N. Simakov, N. M. Pavlovskiy, N. G. Kalashnikov and R. F. Trunin. Shock compressibility of twelve minerals. *Izv. Phys. Solid Earth* 8, 488-492 (1974).
- [9] J. W. Swegle. Irreversible phase-transitions and wave-propagation in silicate geologic materials. *J. Appl. Phys.*, 68, 1563-1579 (1990).
- [10] F. Hörz. Statistical measurements of deformation structures and refractive indices in experimentally shock loaded quartz. *Shock metamorphism of natural materials*. B. M. French and N. M. Short (eds.), Mono Book Corp., Baltimore, 243-254 (1968).
- [11] M. R. Carroll and M. J. Rutherford. Sulfur speciation in hydrous experimental glasses of varying oxidation state: Results from measured wavelength shifts of sulfur X-rays. *Am. Mineralogist*, V 73, 845-849 (1988).
- [12] J. I. Goldstein, D. E. Newbury, P. Echlin, D. C. Joy, A. D. Romig, Jr., C. E. Lyman, C. Fiori and E. Lifshin, *Scanning electron microscopy and X-ray microanalysis: a text for biologists, materials scientists, and geologists*, 2nd edition. Plenum Press, New York (1992).
- [13] S. J. B. Reed, *Electron microprobe analysis*, Cambridge University Press (1975).
- [14] J. B. Brady. Diffusion Data for Silicate Minerals, Glasses, and Liquids, in *Handbook of Physical Constants*, ed. by T. J. Ahrens, Am. Geophys. U. in print.
- [15] D. C. Rubie, C. R. Ross II, M. R. Carroll and S. C. Elphick, Oxygen self-diffusion in $\text{Na}_2\text{Si}_4\text{O}_9$ liquid up to 10 GPa and estimation of high-pressure melt viscosities. *Am. Mineralogist*, V 78, 574-582 (1993)
- [16] J. F. Barnes, D. H. Janney, R. K. London, K. A. Meyer, D. H. Sharp. Further Experimentation on Taylor Instability in Solids. *J. Appl. Phys.* 51, 4678-4679 (1980).

- [17] P. W. Berg and J. L. McGregor, *Elementary Partial Differential Equations*, Holden-Day, San Francisco (1966). large2M. A. Lange and T. J. Ahrens, Shock-induced CO₂ loss from CaCO₃; implications for early planetary atmospheres. *Earth and Planetary Sci. Lett.* 77, 409-418 (1986).
- [18] S. P. Marsh, *LASL Shock Hugoniot Data*, University of California Press, Berkeley (1980).